Physical Modelling in Geotechnics

Effects of previous rainfall on failure mechanism of volcanic embankments under subsequent seismic loadings

T.N. Nguyen, S. Kawamura & T. Inaba
Graduate School of Engineering, Muroran Institute of Technology, Japan

ABSTRACT: This study aims to clarify the effects of previous rainfall on the failure mechanism of the embankments under subsequent earthquakes by physical modelling. A series of the 1g model tests were conducted on embankments constructed from Komaoka volcanic coarse-grained soils using an apparatus that integrated both the spray nozzle and the shaking table. In the experiments; deformation, pore water pressure, saturation degree, and acceleration were monitored and measured to provide an understanding of the mechanical behavior of the model embankment under seismic loadings after rainfall. The results showed that the performance of seismic loadings is strongly affected by the rainfall-induced residual pore water pressure. Determining the water retention condition plays an important role in discussing slope stability. Finally, by comparing the data in this study and those in experiments on rainfall-induced failure after seismic loadings with the same test material, equipment, and procedure; the influence of the impact order of external effect on the slope failure was clarified.

Keywords: slope stability, volcanic soils, rainfall, seismic loadings, physical modelling.

1 INTRODUCTION

Volcanic soil (pyroclastic flow or pyroclastic fall deposits) exists as natural slopes and grounds in many areas around the world, including Japan, and is commonly used as road embankments or backfill. However, because of their intrinsic characteristics, volcanic slopes are extremely prone to become the cause of failures when subjected to disasters. Although research has been made on the mechanical and physical properties of volcanic soils using element tests such as triaxial experiments, studies based on the results of model tests are still quite restricted.

Global warming due to climate change in recent years has resulted in more regular occurrences of heavier-than-expected rainfall, which, when combined with other impacts like cyclic loadings or freeze-thaw actions, has caused unpredictable consequences. Among those complex disasters, earthquake after rainfall is quite common and has always led to massive landslides (e.g., the 2018 Hokkaido Eastern Iburi earthquake that occurred after Typhoon Jebi, the 2004 Niigata Chuetsu earthquake, or the 1968 Tokachi-oki earthquake).

Based on the data of a series of 1g physical model tests, the earthquake-induced failure and mechanical behavior of embankments constructed by Komaoka volcanic coarse-grained soil subjected to previous rainfall were clarified. In particular, the slope stability under post-rainfall earthquakes in this study will be compared with those in the case of the post-rainfall earthquake in (Kawamura et al., 2016). As a result, the influence of the order of external forces on the embankment's collapse mechanism is investigated.

2 TEST MATERIAL AND TEST PROCEDURES

Test material in this study are Komaoka volcanic coarse-grained soils (Spfl) from Shikotsu caldera's ejecta, Hokkaido, Japan (ρ_s = 2.47 g/cm^3, e_{max} = 2.25, e_{min} = 1.21, D_{50} = 0.27mm, Uc = 46, Fc = 27%). Through the results of consolidated undrained triaxial tests for Spfl, (Kawamura et al., 2021) proved the feasibility of using this soil in prototype as the sample of 1g model tests. The similarity laws for the shaking table tests presented in that study are also applied to this study. According to the soil compaction A-c method of JGS 0711-2009, the optimal water content of Spfl w_{opt} is 40.5%. The model slopes were built with a compaction degree of 90% (ρ_d=0.95 g/cm^3). The initial water content was 43%, representing the wetter side of the optimal water content (in practice, the soil is usually compacted on the wetter side around w_{opt} in Japan).

Fig. 1 depicts the test apparatus used in this study. The model soil tank is fitted with 20mm thick tempered glass on the side to allow recording of the slope phenomena and deformation. A one-dimensional vibration loading system was added to the bottom of this tank. The computer-controlled hydraulic cylinder for this system can apply regular wave (sinusoidal shape) with a frequency range of 0.05-5.0Hz, an amplitude of ±50 mm, and a maximum weight of 150 kg. The support system of the spray nozzle can be adjusted to make sure that rainfall is spread over the whole slope, and the valve system manages the intensity of the rainfall.

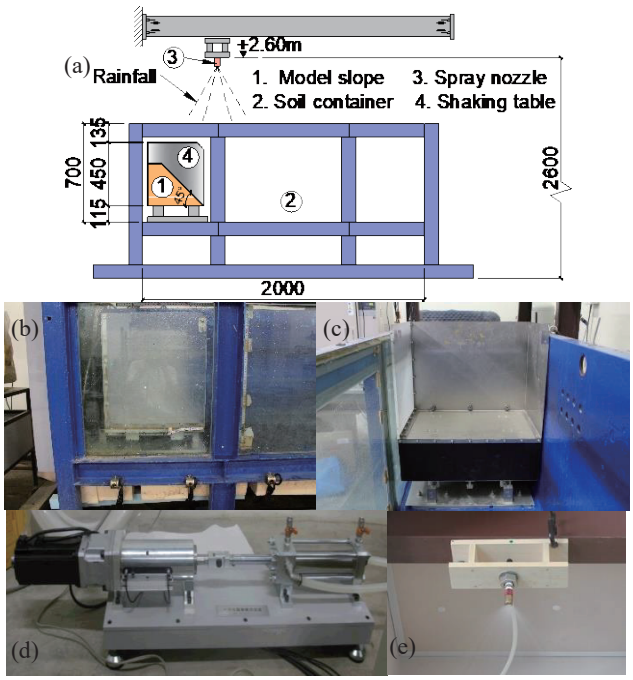

Fig. 1. Test apparatus (a) Overall view (b) Side view (c) Front view (d) 1-dimensional vibration loading device (e) Spray nozzle.

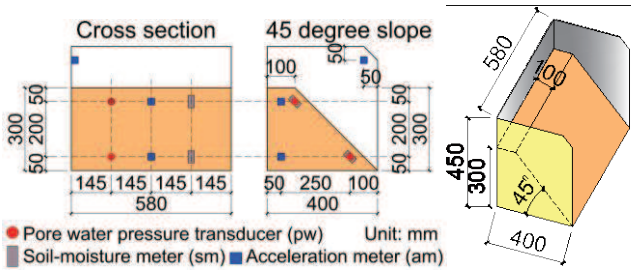

Fig. 2. Model slope and measuring instruments.

The form of the model slopes and the location of measurement gauges are shown in Fig. 2. To understand the slope failure mechanism under post-rainfall earthquakes; pore water pressure, saturation degree, and acceleration were measured, while shear strain was computed from the displacement of kite strings. In this study, the slope failure is determined as the time when the shear strain γ reaches 6% (Kawamura and Miura, 2013). The experimental conditions are listed in Table 1.

Table 1. Test conditions.

Parameters	Value
Slope angle (^{0})	45
Length of base (mm)	400
Initial water content (%)	43
Dry density (g/cm^3)	0.95
Rainfall intensity (mm/h)	100
Acceleration (gal)	280, 320
Number of cycles	20

Given the fact that real earthquakes might happen at any moment following the end of rainfall, seismic loadings in this study were applied to the model slope according to 3 typical cases based on different pore water pressure conditions before earthquakes:

- Case (i): pw1 is higher than pw2;
- Case (ii): pw1 and pw2 reach the lowest value;
- Case (iii): pw2 is higher than pw1.

In which, pw1 and pw2 are the pore water pressure at the upper part and lower part of the slope, respectively.

3 TEST RESULTS AND DISCUSSIONS

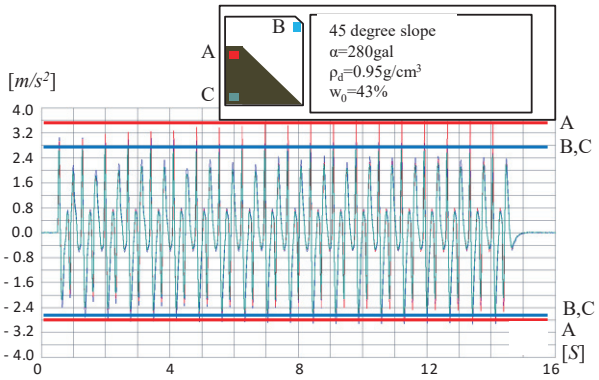

Fig. 3. Accelerations at the basement, crown of the embankment, and shaking table.

Similar to the results of other 1g model tests, the change of pore water pressure Δu in this study is normalized by the initial effective overburden pressure σ_{v0}', and the saturation degree Sr is normalized by its initial value Sr_0. Before post-rainfall earthquake experiments, rainfall-only tests were conducted; the time until failure, in this case, is 1050 seconds (0.29h). The cumulative rainfall up to this failure time is set as the total rainfall amount R_0, R_0 is equal to 29mm (100mm/h x 0.29h). The model slope was firstly subjected to the precipitation of $R=0.5R_0$ before seismic loadings were applied according to cases (i), (ii), and (iii). In Fig. 3, the earthquake input motion used in the experiments is shown through the measured acceleration at the shaking table (point B), the upper part (point A), and the lower part (point C) of the embankment. A common tendency is observed for both the earthquake-only and the post-rainfall earthquake experiments: the maximum acceleration near the crown area of the slope is larger than those at other locations.

The variation of the pore water pressure ratio and saturation degree ratio in the case of (i) are shown in Fig. 4. Because of seepage, the pore water pressure inside the embankment rises immediately when the rain begins. After reaching a certain value, this increase slows down. During rainfall, saturation degree only slightly increases, implying that runoff takes precedence over infiltration at w_0=43%. When the residual pore water pressure is still

high after the rain has stopped for roughly 60 seconds, seismic loadings are applied. As shown in Fig. 4, the pore water pressure at both locations immediately increased when subjected to earthquake, and pw1 placed near the crown of the slope surpassed 1 owing to the response characteristics and quick seismic loadings. The saturation degree, like the pore water pressure, changes rapidly when subjected to earthquakes. The flow deformation at the crown was also confirmed.

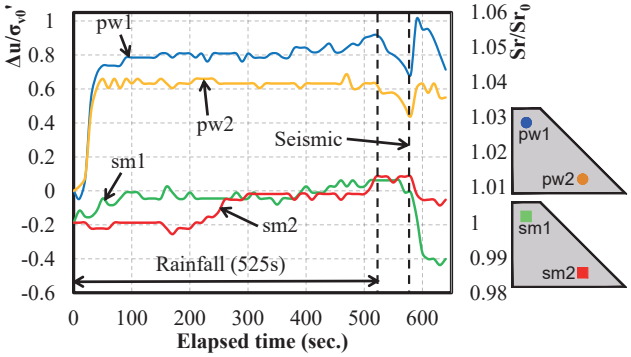

Fig. 4. Change in pore water pressure and degree of saturation in case (i).

Next, with an acceleration of 280 gal in case (ii), the embankment did not collapse as in cases (i) and (iii). As a result, the change in pore water pressure and saturation degree in the embankment until failure in case (ii) is analyzed with an acceleration of 320 gal as presented in Fig. 5. After rainfall stops, the values of pw1 and pw2 decrease over time similar to case (i). When the dissipation period was increased to more than 10 minutes, the pore water pressure at both places decreased to zero, and the earthquake test was performed. Although pw1 and pw2 had been at their lowest before seismic loadings, they changed promptly and exhibited an upward trend after 20 cycles. The pw1 value exceeded 1 and the upper part showed flow deformation. The difference in the failure phenomenon from case (i) is the development of transverse cracks near the crown of the slope. The saturation degree shows almost no change when subjected to earthquakes.

Finally, Fig. 6 depicts the change of pore water pressure and degree of saturation in case (iii). During the 2 hours since the rainfall had stopped, the pore water pressure reduced similarly to case (ii) and then rose again due to the penetration of rainwater and the consolidation over time. When subjected to earthquakes, both excess pore water pressure ratios pw1 and pw2 exceed 1, and the higher values than cases (i) and (ii) were recorded. Flow deformation was observed almost simultaneously in both the upper and lower areas of the embankment. The earthquake-induced cracks are longer and appear both at the upper area and the crown of the slope. Regarding the saturation degree, right after the earthquake was applied, sm1 sharply increased, and sm2 sharply decreased. The failure type of model slope is shown in Fig. 7 with flow deformations and cracks highlighted in cyan and yellow, respectively.

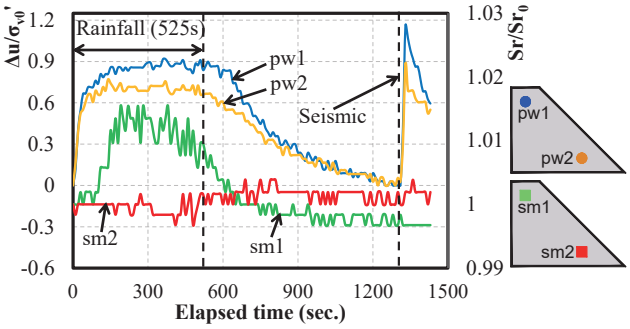

Fig. 5. Change in pore water pressure and degree of saturation in case (ii).

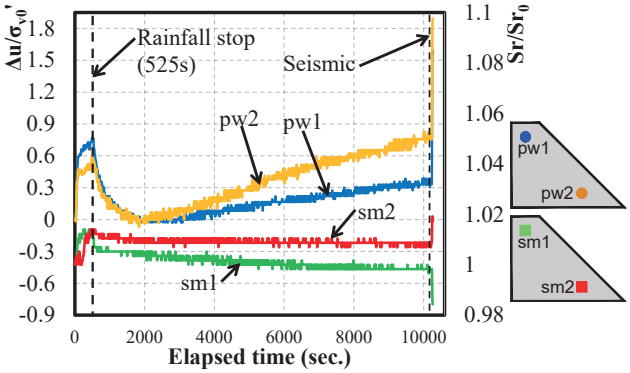

Fig. 6. Change in pore water pressure and degree of saturation in case (iii).

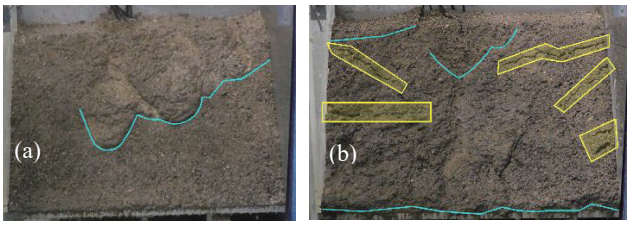

Fig. 7. Model slope at failure (a) case (i) (b) case (ii) & (iii).

Aside from the precipitation of R=0.5R$_0$, other rainfall amount of 0.3R$_0$, 0.6R$_0$, and 0.7R$_0$ were conducted for the model slopes to get different shear strains. Following that, we applied earthquakes and get different failure times. In this study, when a research object is firstly affected by event A and then is collapsed by event B, the failure time ratio is calculated as follows:

$$R_{ft}^{A-B} = T_{fB} / T_{fB0} \quad (1)$$

In which, T_{fB} is the event B-induced failure time of the research object that was subjected to event A in the past, while T_{fB0} is the failure time due to only event B. The smaller the value of the failure time ratio, the greater

© 2022 KOREAN GEOTECHNICAL SOCIETY (KGS), Seoul, Korea, ISBN 978-89-952197-7-5

the effect of event A on the resistance to failure due to event B of the research object. Fig. 8 depicts the relationship between earthquake-induced failure time and the shear strain generated by previous rainfall under various cases of pore water pressure before seismic loadings. As shown in the figure, when the shear strain caused by rainfall increases, the seismic failure time decreases. At the same shear strain, case (ii) has the longest failure time, followed by case (iii), and the failure time in case (i) is the shortest. Although the difference in the time is small, the effect for the case of 37% is more significant than those of 43%. This result implies that the influence of the residual pore water pressure or the dissipation after rainfall cannot be ignored.

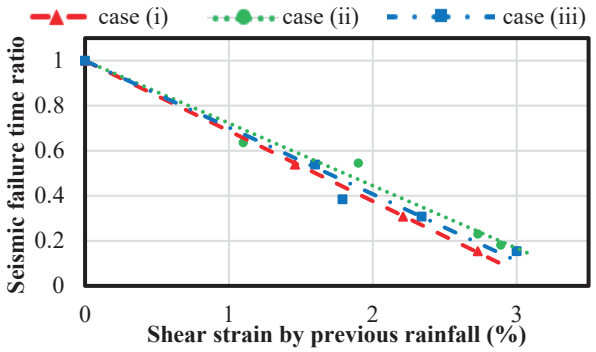

Fig. 8. Relationship between seismic failure time ratio and rainfall-induced shear strain in 3 cases.

Fig. 9 shows the relationship between failure time ratio and shear strain generated by previous external force in this study (case (i)) and the results of earthquakes before rainfall experiments performed by (Kawamura et al., 2016). Different from this study, the failure time ratio when earthquakes are applied first still increases when the shear strain γ increases from 0 to 4%, it only decreases after γ reaches 4%. In particular, at the same shear strain generated, the failure time in this study is shorter compared with post-earthquake rainfall cases.

When seismic loadings are applied first, they raise pore water pressure but also raise soil density because of the compaction effect. As a result, subsequent rainfall will take longer to loosen the soil structure to destabilize the slope. Meanwhile, in the case of post-rainfall earthquakes, rainfall increases the volumetric weight of the soil, leading to the increase of vertical driving force in the slope. Following that, earthquakes not only generate horizontal driving force but also reduce shear strength because pore water pressure due to seismic loading combines with rainfall-induced pore water pressure. These findings highlight the need to properly assess embankments subjected to dual hazards, taking into consideration the impact orders of external forces.

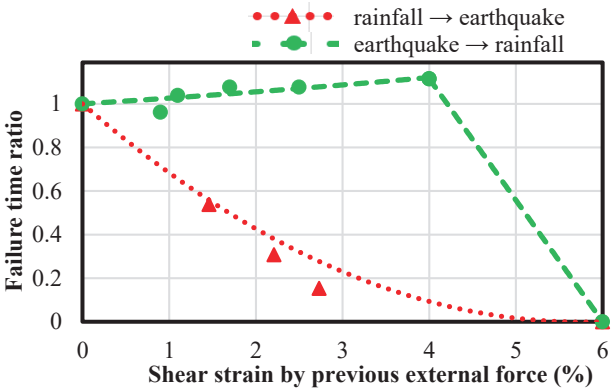

Fig. 9. Relationship between failure time ratio and shear strain generated by previous external forces.

4 CONCLUSIONS

The following conclusions were derived from a series of model experiments in this study:

(1) Residual pore water pressure and water retention conditions inside the embankments after previous rainfall have a great influence on the resistance to subsequent earthquakes.

(2) When embankments are subjected to dual disasters, the slope stability may be various for different orders of earthquake and rainfall even though the preceding received shear strain is similar.

ACKNOWLEDGEMENTS

The authors wish to express their sincere gratitude to Mr. Y. Kusuda and Mr. R. Yamada (Muroran Institute of Technology, Japan). This work was supported by JSPS KAKENHI (A) (Grant Number 20H00266) and JST SPRING (Grant Number JPMJSP2153) in Japan.

REFERENCES

Kawamura, S., & Miura, S. 2013. Rainfall-induced failures of volcanic slopes subjected to freezing and thawing. Soils and Foundations, Vol. 53, Issue 3, 443–461

Kawamura, S., Miura, S., Dao, H. M., & Yamada, R. 2016. Rainfall-Induced Failure of Volcanic Embankments Subjected to Cyclic Loadings in Cold Regions. Geo-China 2016. Geotechnical Special Publication, No.257, 116-123.

Kawamura, S., Miura, S., & Matsumura, S. 2021. Stability Monitoring of Embankments Constructed by Volcanic Coarse-Grained Soil in Snowy-Cold Regions. Journal of Cold Regions Engineering, Vol. 35, Issue 1, p. 04020030